Journal of Alloys and Compounds 516 (2012) 192–200

Contents lists available at SciVerse ScienceDirect

Journal of Alloys and Compounds

journal homepage: www.elsevier.com/locate/jallcom

Correlation between solid fraction and tensile properties of semisolid RAP processed aluminum alloys

Amir Bolouri [a,1], Chung Gil Kang [b,*]

[a] Graduate School of Mechanical and Precision Engineering, Pusan National University, Busan 609-735, Republic of Korea
[b] School of Mechanical Engineering, Pusan National University, Busan 609-735, Republic of Korea

ARTICLE INFO

Article history:
Received 29 August 2011
Received in revised form 8 December 2011
Accepted 12 December 2011
Available online 21 December 2011

Keywords:
Aluminum alloys
Semisolid processing
Mechanical properties
Microstructure

ABSTRACT

Recrystallization and remelting (RAP), a promising route for thixoforming process, was used to process three aluminum alloys, AA2024, AA6061, and A356, under experimental conditions designed to yield various solid fractions (liquid fractions) within the microstructure. The thixotropic microstructures obtained were characterized in detail and linked to the corresponding tensile properties. When the liquid fraction increased (the solid fraction decreased), an initial reduction in the tensile properties was perceived. The lowest tensile properties were obtained at liquid fractions of 35% (610 °C), 25% (623 °C), and 40% (585 °C) for AA2024, AA6061, and A356 alloys, respectively. For the AA6061 and A356 alloys, a further increase in the liquid fraction resulted in improvement of the tensile properties. However, for the AA2024 alloy, the samples could not withstand their own weight at higher liquid fractions that further tensile tests were rendered. It was concluded that for alloys below the liquid fraction corresponding to the minimum tensile properties, the structural properties of interconnected grains (skeletons), and the quenched liquid eutectic phase located at the grain boundaries (liquid film) controlled the fracture behavior. Nevertheless, the nature of the cohesion between the grains and the liquid film was the determining factor in the improvement in the tensile properties that resulted when the liquid fraction was increased to 46% and 60% for the AA6061 and A356 alloys, respectively.

1. Introduction

Semisolid metal processing (SSP) is a near net shape manufacturing process for metals and alloys. The process takes place in the mushy zone of the alloys. Several reviews are available [1–5]. It has been recognized that components fabricated by SSP offer better mechanical properties than conventional castings; the properties of these components are very close to those of forged components. More recently, SSP technique has been employed for processing of metal matrix composites since SSP offers simple, flexible and effective procedure to fabricate large size components [6–9]. In addition, SSP of alloy steels has attracted a considerable attention, because it facilitates the fabrication of complex-shaped steel parts [10,11]. For SSP of alloys, the alloys need to have a microstructure that consists of fine equiaxed grains surrounded by a liquid matrix. This feature offers thixotropic behavior of the alloys in the semisolid state: the alloys flow when sheared but behave like solids when allowed to stand. The solid-like behavior is due to the presence of a solid skeleton of interconnected grains [12,13].

Thixoforming is one branch of SSP in which the initial feedstock material is in the solid state. The process requires a feedstock that exhibits thixotropic behavior when reheated into the semisolid state. One of the most promising routes for preparation of the feedstock for thixoforming is recrystallization and remelting (RAP) process [14,15]. The RAP process is based on warm working (extrusion) of materials below the recrystallization temperature in order to induce sufficient strain energy in the microstructure. Then, when the material is reheated into the semisolid state, recrystallization occurs and the liquid phase penetrates into the grain boundaries of the new subgrains, thereby resulting in equiaxed grains in a liquid matrix [16,17]. Subsequently, when the desired liquid fraction is reached, thixoforming will be conducted.

Previous papers described the detailed microstructural evolution of different alloys in RAP process [16–19]. In addition, microstructure development after different reheating procedures and thixoforming techniques has been the subject of several research works [20–24]. Furthermore, the mechanical properties of parts fabricated by thixoforming processes have been evaluated, and they have been mainly compared with convectional castings [22–29]. However, the results have been influenced by the applied thixoforming conditions and techniques and are thus

* Corresponding author. Tel.: +82 51 510 2335; fax: +82 51 518 1456.
E-mail addresses: amir.bolouri@yahoo.com (A. Bolouri), cgkang@pusan.ac.kr (C.G. Kang).
[1] Postal address: School of Mechanical Engineering, Pusan National University, Busan 609-735, Republic of Korea.

0925-8388/$ – see front matter © 2011 Elsevier B.V. All rights reserved.
doi:10.1016/j.jallcom.2011.12.045

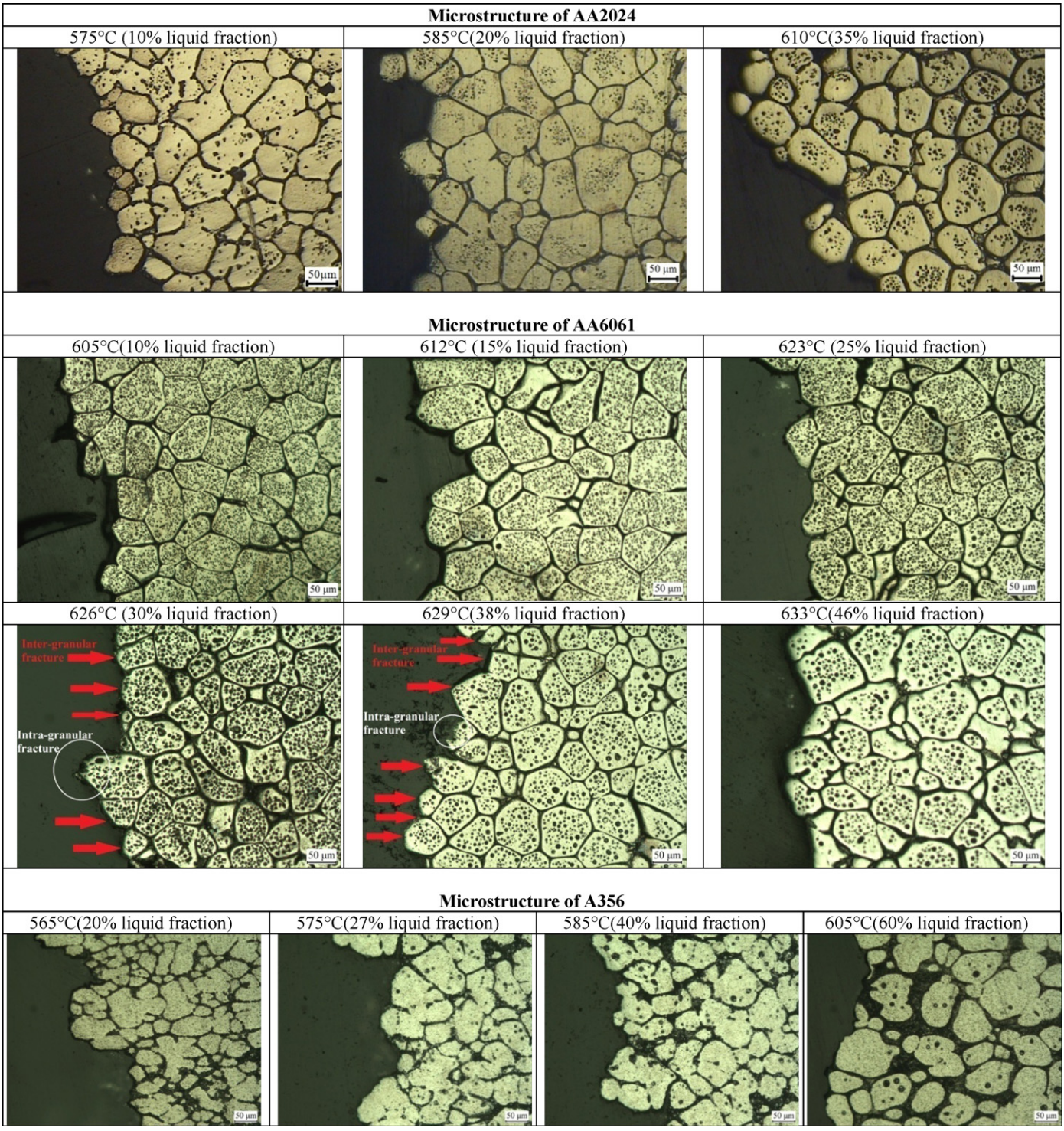

Fig. 1. The microstructures of alloys at different holding temperatures after RAP processing.

valid only for the case studies. On the other hand, the effects of the starting material (feedstock) have only been evaluated from manufacturing points of view, such as for die filling. Different initial conditions of the starting material, such as different solid fractions, could lead to different intrinsic mechanical properties of the starting material. This would dominantly affect the final properties of any fabricated parts. Accordingly, assessing the impact of using feedstock with different initial conditions on the mechanical properties of the semisolid alloys would be of interest. This topic has never been studied. So far, some fundamental knowledge, such as the fracture mechanism during tensile tests and the relationship between the microstructure and the mechanical properties of the semisolid alloys, is still unclear. Some theories that have been developed about the relationship between the microstructure and the mechanical properties of traditionally cast alloys are not applicable to semisolid processed alloys.

The present article is part of a comprehensive study on the effect of microstructural characteristics on the mechanical properties and fracture mechanisms of semisolid processed alloys. The RAP route (without thixoforming) has been employed to prepare

Table 1
The heating temperatures for the alloys.

Alloy	Different heating temperatures (°C)
AA2024	575, 585 and 610
AA6061	605, 612, 623, 626, 629 and 633
A356	565, 575, 585 and 605

samples with different liquid fractions (at different holding temperatures). Thus, both the geometrical effects of the thixoformed parts and the effects of the thixoforming conditions on the tensile properties could be avoided. This offers essential data for evaluating the expected mechanical properties of any fabricated parts as well as the level of the effect of the thixoforming parameters on the final mechanical properties. Using fractographic observation and micrographic examination, the effects of the solid fraction and the structural properties of the equiaxed grains and liquid phase on the tensile properties of AA2024, AA6061, and A356 aluminum alloys have been thoroughly studied and discussed.

2. Experimental procedures

Three different commercially extruded (with an extrusion ratio of 12) starting materials, AA2024, AA6061, and A356 aluminum alloys, were used for this work. The billets were extruded at 440 °C. The alloys were selected to represent the range of major wrought and cast aluminum alloys. For the reheating experiments, disk-like samples 80 mm in diameter and 18 mm in length were machined from the starting billets. In order to monitor the temperature, a hole on the lateral part of the samples was drilled, into which a K-type thermocouple was inserted. Using a resistance furnace, the samples were rapidly heated up to the desired temperature. The average heating rate was 110 °C/min. The samples were then held for 5 min at the desired temperature to allow globularization of the grains and then quenched in water at room temperature. The heating temperatures for each alloy are shown in Table 1.

The tensile test specimens were machined from the quenched disk-like samples and prepared according to ASTM E 8M standards. The tensile specimens were extracted perpendicular to the extrusion direction. The position at which the specimens were machined was the same for all alloys. The tensile test machine loaded the specimens at a 0.008 s^{-1} strain rate. An extensometer was used to exactly measure the elongation of the specimen gauge length. The tensile curves were analyzed to assess the ultimate tensile strength (UTS) and elongation. The reported UTS and elongation values were the average results from three tensile test specimens. The fracture samples were sectioned and prepared according to standard metallographic practices. The samples were etched with Keller solution before they were examined with an optical microscope. Morphological and microchemical characterizations were made by examining the polished side views (profile) of the fractures and the fracture surfaces with a scanning electron microscope (SEM) equipped with an energy dispersive X-ray spectroscopy (EDS). All quantitative measurements were carried out with a minimum of 500 grains in a sample by means of iSolution DT software.

3. Results and discussion

3.1. Microstructural analysis

Fig. 1 shows the typical microstructural evolution and the side views (profiles) of the fracture surfaces of the alloys after the RAP processing at different holding temperatures (solid fractions). When the alloys were heated into the semisolid state, and the temperature reached the solidus temperature of the alloys, remelting started at the grain boundaries [16]. Subsequently, the microstructures of the as-received alloys changed to a nondendritic microstructure mostly consisting of equiaxed solid grains in a matrix of the liquid phase. For each alloy, the microstructural differences among the specimens were mainly based on the liquid fractions and the grain sizes at the various holding temperatures. The variation in the liquid fraction is illustrated in Fig. 2. The liquid fraction was analyzed using the image analyzer software, and the final liquid fraction (f_l) was calculated using the following equation:

$$f_l = \frac{A_{lf}}{A_T} \times 100,$$

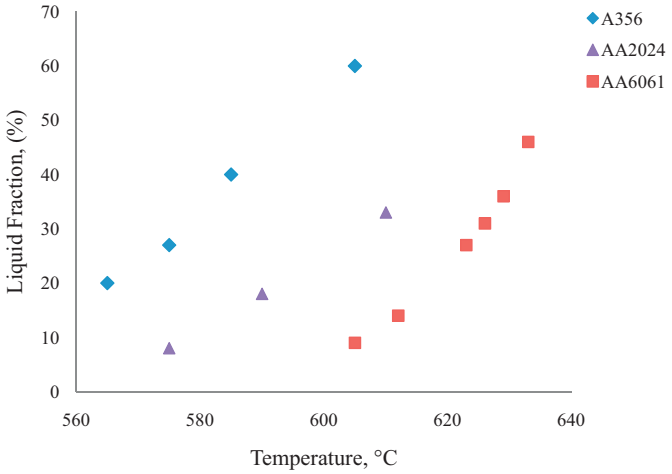

Fig. 2. The variation in liquid fraction versus temperature for the alloys.

where A_{lf} is the total area of the final liquid phase and A_T is the total analyzed area. It was evident from the micrographs and the calculated results that an increase in the holding temperature resulted in a concomitant increase in the liquid fraction and in the thickness of the liquid film located at the grain boundaries. The presence of a large number of entrapped liquid droplets (isolated liquid pockets) inside the grains was a distinct feature of AA2024 and AA6061 wrought alloys from the A356 cast alloy. However, the distributions of the droplets within the AA2024 and AA6061 grains were quite different. For AA6061, the droplets were distributed throughout each grain, while for AA2024, the droplets were mainly observed in the central regions of the grains. Moreover, for AA6061, a low holding temperature (605 °C) resulted in many small liquid droplets that became fewer and larger as the holding temperature increased (high liquid fraction). By contrast, for AA2024, few droplets were observed at a low liquid fraction (at 575 °C), and when the liquid fraction increased, they became greater in number and larger in size.

The solidification shrinkage and porosity are significant structural factors of any casting. It is generally claimed that the improved integrity of SSP castings is attributable to their lower solidification shrinkages compared to those of conventional castings [2]. For thixo-route, reductions in the volumetric shrinkages of as much as 50% have been reported [30,31]. This reduction is due to the presence of solid grains during SSP. Note that in the current study, specimens without evident localized porosity were selected for tensile tests. However, the solidification shrinkage microspores could not be revealed by optical microscopy. The significant effect of solidification shrinkage on the structural properties of the coexisting phases (the grains and liquid film) and its subsequent influence on the tensile properties will be discussed in detail later.

As outlined earlier, according to the microstructural features of the fracture profiles (Fig. 1), the structure components that appeared in the zone of material beneath the fracture surface were globular grains and a quenched liquid phase. In general, the fracture might be considered to be an extension of cracks in the material consisting of the brittle phase (quenched liquid phase) and the ductile second phase (grains). Note that the liquid phase was in the form of a liquid film located at the grain boundaries and in the form of liquid droplets within the grains. Since the rare evidence of fractures within the grains (intragranular fracture) was only detected for AA6061 alloy at 626 °C and 629 °C, it seems that intergranular fracture mainly occurred (Fig. 1). Furthermore, the marked absence of intragranular fractures might imply that the interface cohesion forces between the grains and the liquid film and/or the cohesion force of the liquid film itself (intercrystalline fracture) were lower

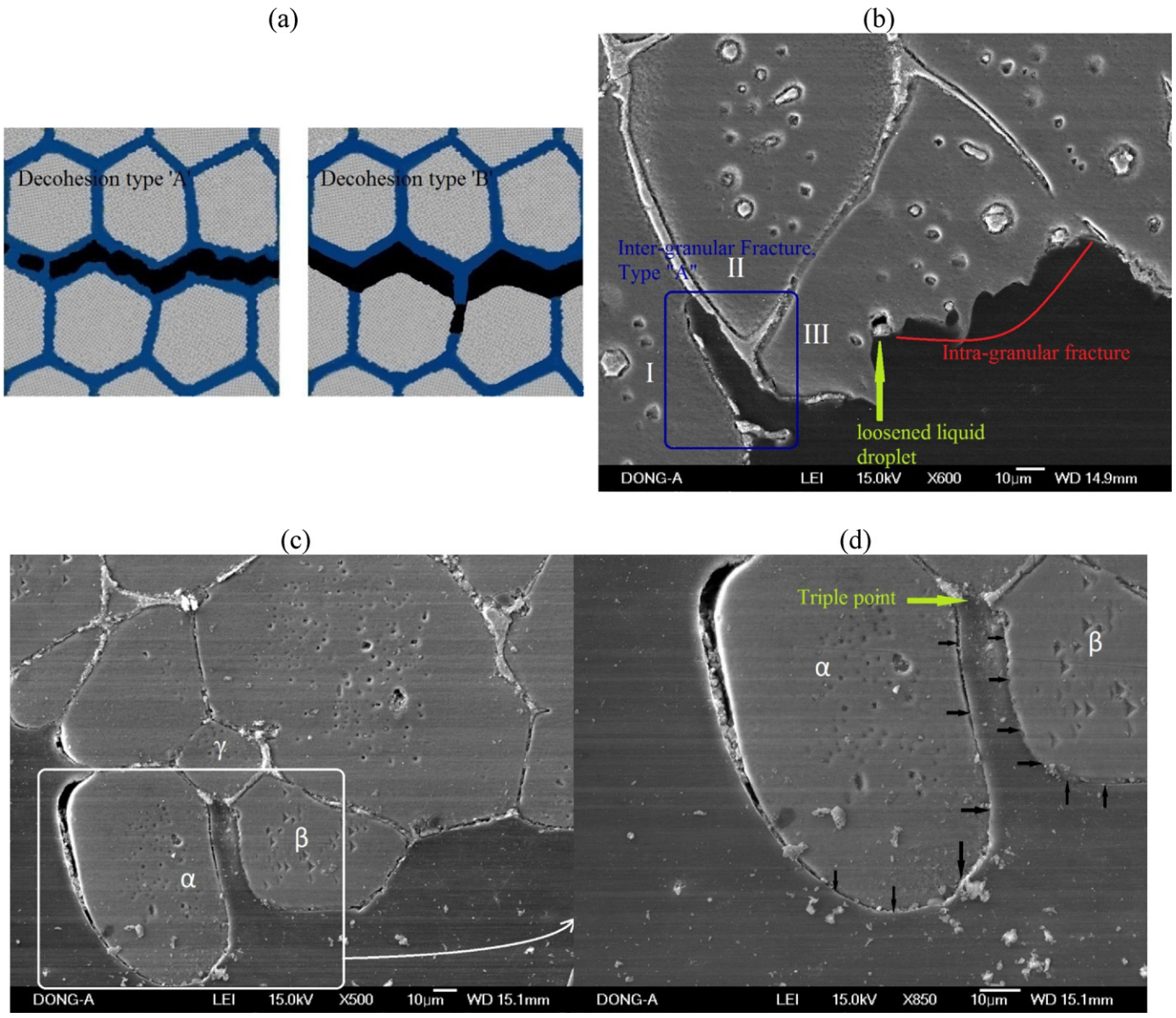

Fig. 3. (a) A schematic for inter-granular fractures decohesion type 'A' and 'B' in which blue color represents the eutectic phase. SEM pictures of fracture profiles (b) AA6061at 629 °C (38% liquid fraction), (c, d) AA2024 at 590 °C (20% liquid fraction). The interface for decohesion type 'B' is shown by arrows (in black) for grains labeled α and β. (For interpretation of the references to color in this figure legend, the reader is referred to the web version of the article.)

than the force needed for decohesion within the globular grains [32,33].

A study on the tensile properties of thixoformed ZA27 alloy by Chen et al. [34] showed that the average grain size and the liquid fraction could strongly affect the tensile properties. In addition, fine equiaxed grains are generally desired, because they provide the best combination of strength and ductility by maximizing the grain boundary surface area and more finely distributing the grain boundary constituents [35]. However, in the current study, the grain size varied throughout the microstructure, which might make it difficult to logically evaluate the fracture behavior according to the grain size. Nevertheless, the smallest average grain size was achieved at the lowest liquid fractions (the lowest holding temperatures): 48 μm, 56 μm, and 65 μm for A356, AA2024, and AA6061, respectively. It is also worth mentioning that the average grain size and solidification shrinkage depend on the liquid fraction. Consequently, it would be of interest to evaluate the fracture behavior according to the liquid phase fraction (solid fraction) [30], which may result in useful conclusions. Note that in this study, the detailed effects of the intermetallic phase on the fracture behavior will not be examined.

According to the fracture profiles in Figs. 1 and 3, with the exception of the intragranular fractures, for the intergranular fractures, two typical types of decohesion could be classified: (A) propagation of cracks through the liquid film located at grain boundaries (intercrystalline fracture of the liquid film) and (B) direct decohesion from the interface between the grains and the liquid film. In other words, type A depends on the cohesion force of the quenched liquid film (quenched eutectic phase) while type B depends on the interface cohesion force between grains and the quenched eutectic phase. A schematic for decohesion types A and B is shown in Fig. 3(a), in which the liquid film is indicated in blue. For AA6061 alloy, typical evidence of decohesion type A, together with the intragranular fracture from the liquid droplets, is clearly shown in Fig. 3(b). The liquid film at the grain boundaries and the liquid droplets appeared as a bright gray color in the SEM pictures.

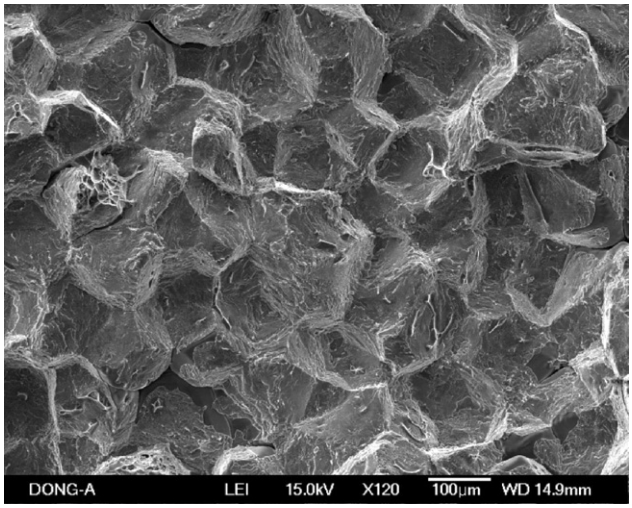

Fig. 4. SEM fractograph of AA6061 at 626 °C (25% liquid fraction).

Fragments of the liquid film on the surfaces of the grains marked I, II, and III were observed, which indicated that the crack propagated through the liquid film. Furthermore, for the intragranular fracture, a loosened liquid droplet in the grain marked III was the most interesting feature of the picture (Fig. 3b). It seems that the holes where the droplets were formed were fully filled with the liquid phase. However, during the solidification, because of the simultaneous effects of the solidification shrinkage and the absence of liquid feeding to the isolated liquid pockets, the liquid droplets might lose their interface cohesion with the solid phase. Subsequently, the holes could act as stress concentration points. This might alter the fracture behavior under specific conditions. For AA2024 alloy, Fig. 3(c) and (d) clearly shows particular evidence of decohesion type B: the rupture occurred at the triple point of the grains labeled α, β, and γ, and it was followed by decohesion of the liquid film from the interfaces of grains α and β. In other words, the liquid film located at the grain boundary between grains α and β (clearly shown in the picture in Fig. 3d) was completely detached during the fracture. Furthermore, a typical debonding characteristic of the fracture could clearly be observed from the SEM fractograph of the tensile-fractured AA6061 alloy specimen in Fig. 4. It is evident from Fig. 4 that grains were detached from the quenched liquid film (grain boundaries) without undergoing remarkable plastic deformation. For all the reasons discussed in this section, it could be supposed that the characteristics of the quenched eutectic phase and nature of the interface cohesion between the coexisting phases (the grains and the quenched liquid phase) have a dominant effect on the fracture behavior of RAP processed alloys.

3.2. Tensile properties

In Fig. 5, the ultimate tensile strength (UTS) and elongation values are reported and compared for alloys with different liquid fractions. As a general trend, an increasing in liquid fraction caused the UTS and elongation values to initially decrease. This decrease was very apparent for AA2024 alloy, in which the UTS and elongation values monotonically decreased. However, for AA6061 and A356, at liquid fractions up to about 15% and 27%, respectively, the UTS and elongation values remained constant, but they then distinctly decreased until the liquid fractions reached 25% and 40%, respectively. On the other hand, it appears that the elongation exhibited a sensitive dependence on the liquid fraction. For AA6061, up to 25% liquid fraction, the elongation value fluctuated at a level of 1.4–2.1%, which implies a quite brittle fracture. However, for A356 the elongation dramatically decreased from

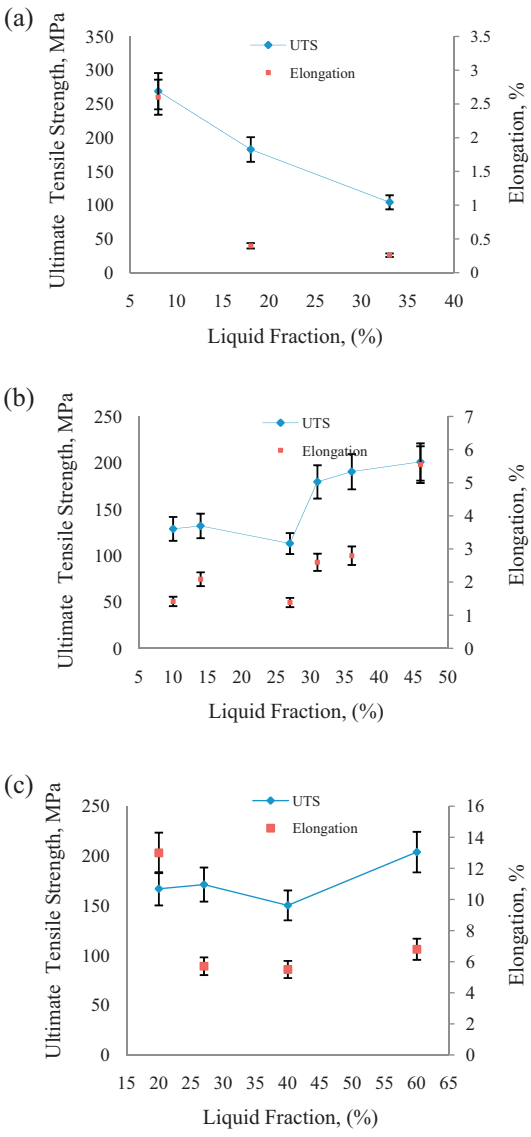

Fig. 5. The ultimate tensile strength and elongation versus liquid fraction during RAP processing for (a) AA2024, (b) AA6061 and (c) A356 alloys. Note that the tensile tests repeated for three times at each liquid fraction. An error of ±10% has been shown on the graphs.

13% (at 20% liquid fraction) to 5.7% (at 27% liquid fraction) and then remained almost constant at 40% liquid fraction. Interestingly, further increases in the liquid fractions from 25% and 40% (the critical liquid fractions) to higher liquid fractions of 46% and 60% for AA6061 and A365 alloys, respectively, resulted in improvement of the tensile properties. Note that for AA2024, the tensile experiments were conducted only at liquid fractions of 10%, 20%, and 35%, since the reheating experiments at higher liquid fractions failed; the samples with higher liquid fractions could not withstand their own weight [36].

For AA2024, sharp drops in the UTS and elongation values occurred when the liquid fraction increased. This trend implies a potentially detrimental effect of high liquid fractions on the tensile properties. The highest UTS and elongation values were obtained at the lowest liquid fraction (10%). It is worth noting that the elongation values of 0.4% and 0.26% obtained at 20% and 35% liquid fractions, respectively, were very small (and negligible) compared to the elongation value (2.7%) at 10% liquid fraction. Thus, at the former liquid fractions fully brittle fractures (0.4% and 0.26% elongations) occurred, while at the latter a quite small amount of plastic

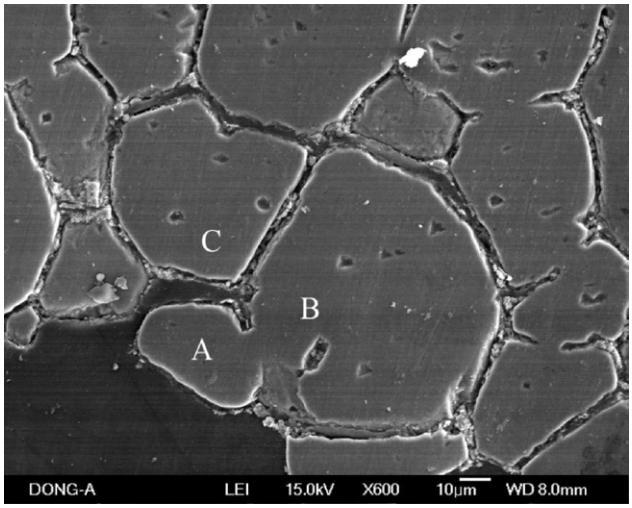

Fig. 6. SEM pictures of fracture profiles for AA2024 at 575 °C (10% liquid fraction).

deformation happened during the fracture. In addition, for A356 alloy, the elongation value changed in a similar way when the liquid fraction increased from 20% to 40% (below the critical value): the highest elongation value (13%) was obtained at the lowest liquid fraction (20%), and it descended considerably to a low value of 5.5% at 40% liquid fraction. Studying the reasons for the differences in the tensile properties, particularly the elongation values at different liquid fractions, could introduce new concepts, as there is no research in this area yet.

As shown in Fig. 1, the distinct microstructure of the alloys at 10% and 20% liquid fractions (for AA2024 and A356, respectively) in which the grains appeared to be mostly interconnected might be the key point for explaining the tensile behavior of the alloys while at higher liquid fractions (up to 35% and 40% for AA2024 for A356, respectively) the solid grains were distinctly separated by the liquid phase (Fig. 1). In general, in the semisolid state of the alloys, the globular grains are loosely interconnected, forming a structural skeleton, and cannot be considered as isolated spheres [12,13,37]. The skeleton in the semisolid alloys is a result of the connections between grains through solid–solid grain boundaries (which will now be referred to as the necks) and ultrathin wetted grain boundaries. The former can be clearly seen in Fig. 1 at high solid fraction of alloys, but the latter is very difficult to quantify and will not be discussed here. Consequently, the higher elongation (plastic deformation) and UTS values for AA2024 and A356 alloys at liquid fractions of 10% and 20% compared to those at liquid fractions of 35% and 40%, respectively, could partially contribute to the revealing effect of the skeletons (interconnected grains) and the large number of necks among the grains at the lowest liquid fraction (Fig. 1). For instance, a typical shearing of a neck between two grains is clearly shown in Fig. 6 (for AA2024 at 10% liquid fraction). Obviously, decohesion between the grains marked "A" and "C" has occurred, but the shearing of grains through the neck (between grains "A" and "B") has given rise to plastic deformation. Note that the evaluation of necking at different holding temperatures could be very complicated [37]. A higher holding temperature might result in melting of many initial necks and coarsening of just a few necks. This might weaken the effect of the skeleton on the mechanical properties of the semisolid alloy. Furthermore, note that the decrease in the UTS values for AA6061 alloy occurred at 25% liquid fraction, presumably, which could also be partially attributed to the weakening in the structure of the skeletons.

Despite the effect of the necks on the tensile properties, the characteristics of the liquid phase (eutectic phase) appeared to dominantly influence the tensile properties of the semisolid alloys [38]. The results of the quantitative energy-dispersive X-ray spectroscopy (EDS) analyses at grain boundaries of the AA2024 and AA6061 alloys are shown in Fig. 7. The increased concentration of alloying elements at the grain boundaries confirmed that the liquid film is the liquid eutectic phase [16]. As shown in Fig. 7, EDS analyses revealed that when liquid fraction increased, the alloying elements were enriched in the quenched eutectic phase located at the grain boundaries [39]. This implies that a network of intermetallic particles formed and increased in amount as the liquid fraction increased. According to the literature and EDS analyses, it seems that the major intermetallic phases for AA2024 are Al_2Cu and Al_2CuMg, and those for AA6061 are Mg_2Si and AlFeSi [40–42]. The formation of intermetallic compounds could potentially lead to the reduction in the tensile strengths of the semisolid processed alloys [31,38]. However, an improvement of the tensile properties achieved by applying different solution and aging post-heat treatments (such as T6) has been reported for semisolid wrought aluminum alloys by other authors [43–45]. All these studies aimed to dissolve the intermetallic phases formed in the eutectic phase located at grain boundaries (liquid film). Liu et al. [23,38] have conducted an extensive study regarding the effect of post-heat treatments (T4, T5, and T6) on the tensile properties of semisolid processed 2014 aluminum alloy. They claimed that after the optimized post-heat treatments, the tensile properties of the alloy were much improved. However, the UTS and the elongation to fracture of the semisolid processed alloy were still poor compared to those of the forged 2014 target. No explanation for these results has been provided. This clearly implies that the tensile properties of semisolid alloys are not only dependent on the characteristics of quenched eutectic phase. Interestingly, according to the evidence in this study, the tensile properties of the semisolid processed alloys, particularly the elongation, also were significantly influenced by the structural properties of the coexisting phases, such as skeletons and interface cohesion between two coexisting phases. In other words, the tensile properties of semisolid alloys are just partly owing to the characteristics of the eutectic phase. Thus, the recovery and improvements in the tensile properties that can be achieved by applying only the post-heat treatments (T4, T5, and T6) are finite. In addition, permanent changes in the tensile properties of semisolid alloys with different liquid fractions might occur because of their different structural properties, such as the different numbers and sizes of necks. A permanent change could not be compensated by any of the post-heat treatments. For this reason, semisolid alloys with different liquid fractions result in various tensile properties even after post-heat treatments [44,45].

If the liquid fraction is increased, the solidification shrinkage will increase [30], and in the absence of appropriate feeding for the liquid film at the grain boundaries, the shrinkage might result in two major defects: (1) micropores within the liquid film and/or (2) loose interface cohesion between the grains and the liquid film. In either case, the mechanical properties of the material would be damaged. Clear evidence of micropores within the liquid film is shown for AA2024 alloy at 35% liquid fraction (Fig. 8a) and for AA6061 alloy at 25% liquid fraction (Fig. 8b). However, as estimated by an Archimedes test, the level of porosity stayed fairly constant at around 0.9–1.5% at the investigated liquid fractions of the alloys. This implies that the tensile properties might be independent of the level of porosity. The same discussion is asserted for thixo-route process of SSP at the solid fractions above 50% [31,46]. Therefore, the interface cohesion between the coexisting phases seems to be the essential factor determining how the tensile properties change. In this study, the interface cohesion is deemed to be a structural effect of the liquid film. The main conclusion to be drawn from this discussion is that the tensile properties of the semisolid alloy are partly due to the structural properties of the skeleton, which consists of interconnected equiaxed grains, and the liquid film, which

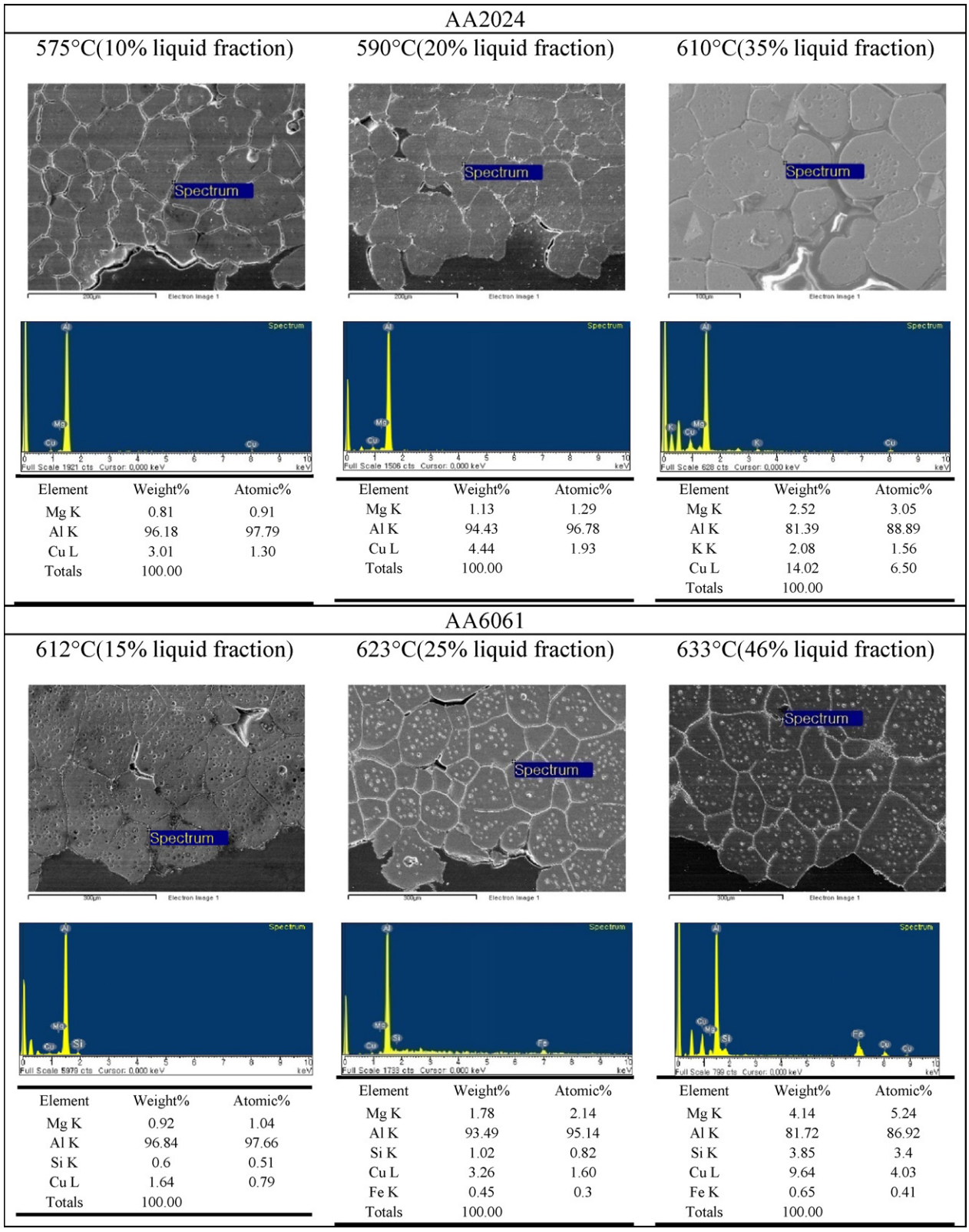

Fig. 7. EDS analyses for AA2024 and AA6061 alloys at different temperatures.

acts as the binder of the skeleton. These structural properties cannot be altered by post-heat treatments, hence the importance of the material processing conditions.

The tensile properties of A6061 and AA356 alloys experienced an initial descent followed by an ascent to the maximum values (Fig. 5). The reasons for the initial decrease have been comprehensively discussed earlier in this section. However, the subsequent ascent was a unique and interesting feature, as it has never before been reported. For AA6061, when the liquid fraction increased from 30% to 38% (at 626 °C and 629 °C), as shown in Figs. 1 and 3,

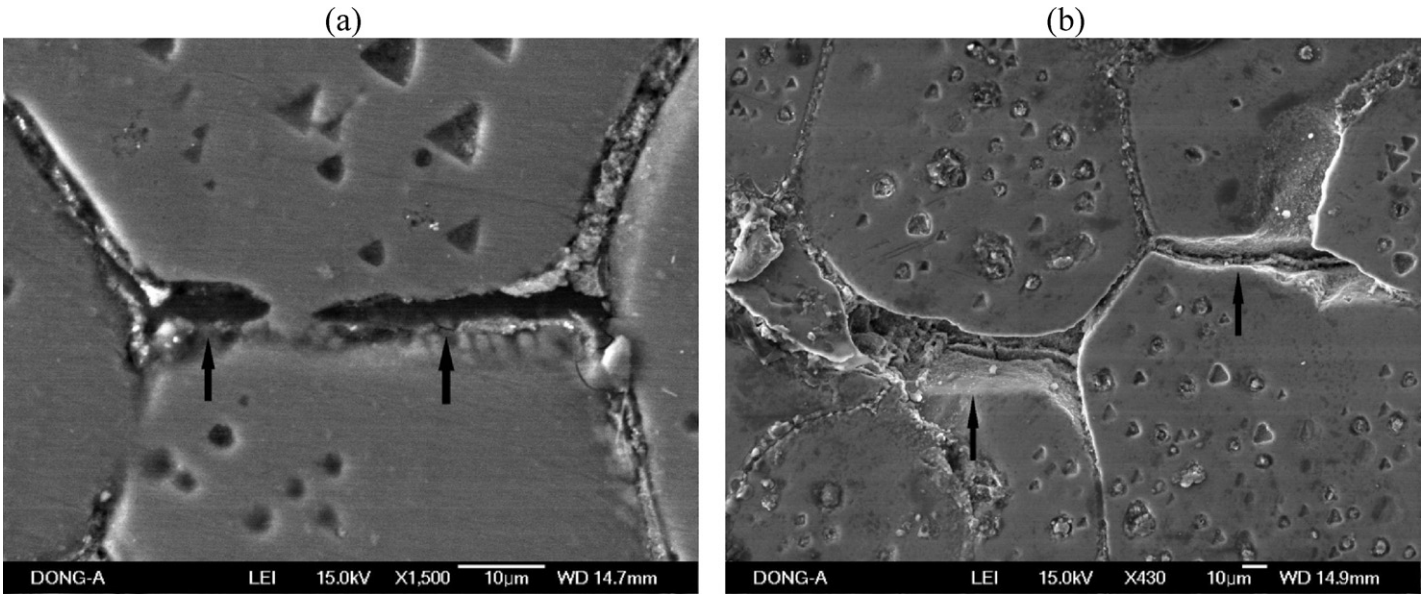

Fig. 8. SEM picture of microstructure for (a) AA2024 at 610 °C (35% liquid fraction) and (b) AA6061 at 623 °C (25% liquid fraction). Micropores are indicated by arrows.

the fractures changed from being only intergranular to featuring shearing of the grains (intragranular fractures). The shearing of the grains might occur through the necks and/or through the grains. In addition, the increase in strength (UTS) of the alloy was accompanied by a simultaneous increase in the elongation (ductility) value. This was especially evident for the AA6061 alloy with a 46% solid fraction. The increase in elongation results from the high level of plastic deformation that occurred in the microstructure. Since the microstructure consisted of a brittle quenched liquid phase and grains, a sound assumption would be that the deformation occurred in the grains rather than in the brittle phase. Evidence for deformation of a grain is clearly noticeable in Fig. 3(a) for the grain marked I: the decohesive surface of grain I with the curved shape in the picture indicates a deformed grain. Therefore, it is fair to conclude that the nature of the cohesion between the coexisting phases has improved. More specifically, the interface cohesion between the quenched eutectic phase and the grains was strong enough that it accommodated the tensile stress and transferred the stress to the grains, causing their deformation and shearing. In Fig. 9, for AA6061 alloy at 46% liquid fraction, clear evidence for the formation of a continuous liquid film at the grain boundaries is shown. The presence of a high liquid fraction provided the appropriate feeding for the eutectic phase located at grain boundaries, thereby diminishing the deleterious effects of the solidification shrinkage on the tensile properties. This could be the main reason for the large improvement in the interface cohesion characteristics. Moreover, this discussion is supported by the rarity of evidence for micropores throughout the liquid film.

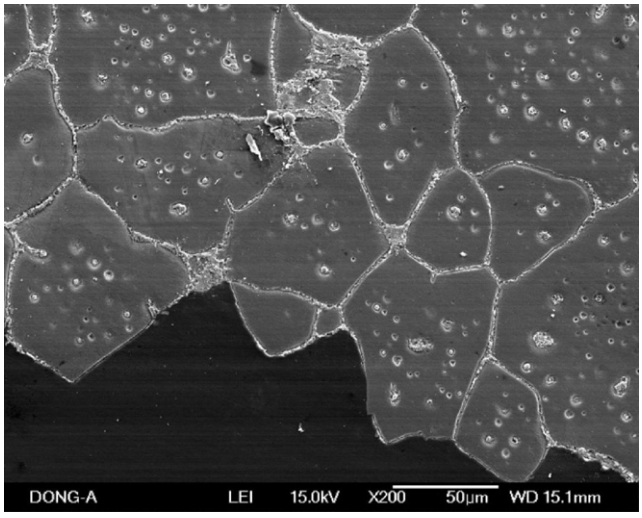

Fig. 9. SEM picture of microstructure for AA6061 at 633 °C (46% liquid fraction).

For A356 alloy, the increasing level of alloying elements such as Si, Mg, Fe, and Mn in the liquid film with increasing liquid fraction was confirmed by EDS analyses. It is expected that some intermetallic phases, such as Mg_2Si, Al_5FeSi, and $Al_{15}(Mn, Fe)_3Si$ were formed [40,47]. In addition, as mentioned earlier, the concentration of alloying elements drastically increased for AA6061 alloy when the liquid fraction increased (Fig. 7). Thus, it could be deduced that for AA6061 and A356 alloys, the presence of intermetallic phases has been increased. This could potentially give rise to the reduction in the tensile strengths. Nevertheless, as discussed earlier, when the liquid fraction reached the critical values of 25% and 40% for AA6061 and A356, respectively, further increases in the liquid fraction led to improvements of the tensile properties. Therefore, it might be assumed that when the critical liquid fraction was reached, the tensile properties of the semisolid alloy became independent of the presence of the intermetallic phase. This clearly confirms the importance of the features of interface cohesion (the structural properties) of the coexisting phases in the fracture behavior of semisolid alloys. However, the morphology, size, and distribution of the intermetallic phases must be investigated thoroughly in order to reveal any related effects. This would require a new approach in the design of experiments for further research.

4. Conclusions

For AA2024, AA6061, and A356 alloys, samples with different liquid fractions were prepared by RAP processing for tensile tests. Optical microstructural observations revealed that the structure components present in the zone of material beneath the fracture surface were globular grains and a quenched liquid eutectic phase. It appeared that intergranular fractures mainly occurred in the samples. Two typical decohesion characters were classified in the fractures: (A) intercrystalline fracture of the

quenched liquid eutectic phase located at the grain boundaries (liquid film) and (B) direct decohesion at the interface between the grains and liquid film.

As the liquid fraction increased, the strength and ductility of the alloys noticeably decreased initially. This was very evident for AA2024 alloy. However, a further increase in the liquid fraction resulted in an increase in the strength of the semisolid AA6061 and A356 alloys that was also accompanied by a simultaneous increase in the ductility. For AA2024 alloy, the samples with higher liquid fractions failed during the RAP processing, which made it impossible to conduct a tensile test.

The fracture mechanism depended on the liquid phase fraction within the thixotropic microstructure. The weakening effect of the skeleton (interconnected grains) was presumed to be the reason for the initial decrease in the tensile properties caused by the increasing liquid fraction. On the other hand, the improvement in the tensile properties of the alloys was attributed to the improvement of the cohesion strength between the coexisting phases. Specifically, it was supposed that the interface cohesion force between the grains and liquid film was high enough that the tensile stress was transferred to the grains, resulting in their deformation.

It was postulated that the interface cohesion between the grains and the liquid film was the determining factor that controlled the tensile properties of the semisolid RAP processed alloys.

Acknowledgments

This work was supported by the National Research Foundation of Korea (NRF) grant funded by the Korea government (MEST) (No. 2009-008/099) and (2011-0030665) of MEST.

References

[1] P. Kapranos, P.J. Ward, H.V. Atkinson, D.H. Kirkwood, Mater. Des. 21 (2000) 387–394.
[2] M.C. Flemings, Metall. Mater. Trans. A 22 (1991) 269–293.
[3] D.H. Kirkwood, Int. Mater. Rev. 39 (1994) 173–189.
[4] Z. Fan, Int. Mater. Rev. 47 (2002) 49–85.
[5] H.V. Atkinson, Prog. Mater. Sci. 50 (2005) 341–412.
[6] S.A. Sajjadi, M. Torabi Parizi, H.R. Ezatpour, A. Sedghic, J. Alloys Compd. 511 (2012) 226–231.
[7] H. Zhang, L. Geng, L. Guan, L. Huang, Mater. Sci. Eng. A 528 (2010) 213–218.
[8] K.B. Nie, X.J. Wang, K. Wu, L. Xu, M.Y. Zheng, X.S. Hu, J. Alloys Compd. 509 (2011) 8664–8669.
[9] L.-N. Guan, L. Geng, H.-W. Zhang, L.-J. Huang, Trans. Nonferrous Met. Soc. China 21 (2011) s274–s279.
[10] J. Hana, A. David, M. Bohuslav, J. Alloys Compd. 504S (2010) S500–S503.
[11] A. Rassili, H.V. Atkinson, Trans. Nonferrous Met. Soc. China 20 (2010) a1048–a1054.
[12] P. Kapranos, D.H. Kirkwood, C.M. Sellars, H.E. Exner, V. Schumacher (Eds.), Proceedings EUROMAT 1989 Conference, Deutsche Gesellschaft fu¨r Metallkunde, Berursel, Germany, 1989, pp. 165–168.
[13] E. Tzimas, A. Zavaliangos, Mater. Sci. Eng. A 289 (2000) 228–240.
[14] K.P. Young, C.P. Kyonka, F. Courtois, Fine Grained Metal Composition, United States Patent No. 4415374, 1983.
[15] D.H. Kirkwood, C.M. Sellars, L.G. Elias-Boyed, Thixotropic Materials, European Patent No. 0305375 B1, 1992.
[16] H.V. Atkinson, k. Burke, G. Vaneetveld, Mater. Sci. Eng. A 490 (2008) 266–276.
[17] S.G. Shabestari, M. Ghanbari, J. Alloys Compd. 508 (2010) 315–319.
[18] A. Bolouri, M. Shahmiri, C.G. Kang, J. Alloys Compd. 509 (2011) 402–408.
[19] J. Jiang, Y. Wang, J. Qu, Z. Du, Y. Sun, S. Luo, J. Alloys Compd. 497 (2010) 62–67.
[20] Y. Birol, J. Alloys Compd. 473 (2009) 133–138.
[21] Q. Chen, Z. Zhao, Z. Zhao, C. Hu, D. Shu, J. Alloys Compd. 509 (2011) 7303–7315.
[22] S. Chayong, H.V. Atkinson, P. Kapranos, Mater. Sci. Technol. 20 (2004) 490–496.
[23] D. Liu, H.V. Atkinson, P. Kapranos, W. Jirattiticharoean, H. Jones, Mater. Sci. Eng. A 361 (2003) 213–224.
[24] E.R. de Freitas, E. Ferracini Jr., M. Ferrante, J. Mater. Process. Technol. 146 (2004) 241–249.
[25] E. Parshizfard, S.G. Shabestari, J. Alloys Compd. 509 (2011) 9654–9658.
[26] H.A. Patel, D.L. Chen, S.D. Bhole, K. Sadayappan, J. Alloys Compd. 496 (2010) 140–148.
[27] S. Chayong, H.V. Atkinson, P. Kapranos, Mater. Sci. Eng. A 390 (2005) 3–12.
[28] S.G. Shabestari, E. Parshizfard, J. Alloys Compd. 509 (2011) 7973–7978.
[29] C.G. Kang, P.K. Seo, S.S. Kang, J. Mater. Process. Technol. 176 (2006) 32–40.
[30] R.F. Decker, R.D. Carnahan, R. Vining, E. Eldener, Proceedings of the 4th International Conference on Semisolid Processing of Metals and Alloys, Sheffield, 1996, pp. 221–224.
[31] F. Czerwinski, A. Zielinska-Lipiec, P.J. Pinet, J. Overbeeke, Acta Mater. 49 (2001) 1225–1235.
[32] M. Warmuzek, Aluminum-Silicon Casting Alloys Atlas of Microfractographs, ASM International, 2004.
[33] M.F. Ashby, C. Ghandi, M.R. Taplin, Acta Metall. 27 (1979) 699–729.
[34] T.J. Chen, Y. Hao, J. Sun, Y.D. Li, Mater. Sci. Eng. A 382 (2004) 90–103.
[35] S. Avner, Introduction to Physical Metallurgy, McGraw-Hill, 1964.
[36] H.-S. Kim, I.C. Stone, B. Cantor, J. Mater. Sci. 43 (2008) 1292–1304.
[37] N. Limodin, L. Salvo, M. Suéry, M. DiMichiel, Acta Metall. 55 (2007) 3177–3191.
[38] D. Liu, H.V. Atkinson, P. Kapranos, H. Jones, J. Mater. Sci. 39 (2004) 99–105.
[39] Y. Birol, J. Mater. Process. Technol. 211 (2011) 1749–1756.
[40] L. Backerud, G. Chai, J. Tamminem, Solidification Characteristics of Al alloys, vol. 2, Foundry Alloys, AFS/Skan Aluminium, 1990.
[41] G. Sha, K.A.Q. O'Reilly, B. Cantor, J. Worth, R. Hamerton, Mater. Sci. Eng. A 304–306 (2001) 612–616.
[42] G. Sha, K.A.Q. O'Reilly, B. Cantor, J.M. Titchmarsh, R.G. Hamerton, Acta Metall. 51 (2003) 1883–1897.
[43] W.A.N.G. Wei-wei, J.I.A. Bin-bin, L.U.O. Shou-jing, Trans. Nonferrous Met. Soc. China 19 (2009) s337–s342.
[44] C.G. Kang, S.W. Youn, P.K. Seo, J. Mater. Process. Technol. 159 (2005) 330–337.
[45] H.-M. Guo, X.-J. Yang, M. Zhang, Trans. Nonferrous Met. Soc. China 18 (2008) 555–561.
[46] D. Ghosh, K. Kang, C. Bach, J.G. Roemer, Proceedings of the 34th Anniversary Congregation of Metallurgists, Recent Metallurgical Advances in Light Metals Industries, Canada, 1995, pp. 473–479.
[47] A.M. Kliauga, M. Ferrante, Acta Metall. 53 (2005) 345–356.